Transport phenomena in microchannel reactors for proton-exchange membrane fuel cell applications

Christopher Brown [a], Junjie Chen [a, b, c, *]

[a] Department of Mechanical and Aerospace Engineering, College of Engineering, University of California, Davis, California, 95616, United States

[b] Department of Automotive Engineering, School of Mechanical and Automotive Engineering, South China University of Technology, Guangzhou, Guangdong, 510641, P.R. China

[c] Department of Energy and Power Engineering, School of Mechanical and Power Engineering, Henan Polytechnic University, Jiaozuo, Henan, 454000, P.R. China

* Corresponding author. E-mail address: junjiem@tom.com

Abstract

Direct oxidation of fuels such as methanol in proton-exchange membrane fuel cells at practical current densities with acceptable catalyst loadings is not as economically attractive as conversion of methanol fuel to a hydrogen-rich mixture of gases via steam reforming and subsequent electrochemical conversion of the hydrogen-rich fuel stream to direct current in the fuel cell. The potential of methanol reforming systems to greatly improve productivity in chemical reactors has been limited, due in part, to the effect of mass transfer limitations on the production of hydrogen. There is a need to determine whether or not a microchannel reforming reactor system is operated in a mass transfer-controlled regime, and provide the necessary criteria so that mass transfer limitations can be effectively eliminated in the reactor. Three-dimensional numerical simulations were carried out using computational fluid dynamics to investigate the essential characteristics of mass transport processes in a microchannel reforming reactor and to develop criteria for determining mass transfer limitations. The reactor was designed for thermochemically producing hydrogen from methanol by steam reforming. The mass transfer effects involved in the reforming process were evaluated, and the role of various design parameters was determined for the thermally integrated reactor. In order to simplify the mathematics of mass transport phenomena, use was made of dimensionless numbers or ratios of parameters that numerically describe the physical properties in the reactor without units. The results indicated that the rate of the reforming reaction is limited by mass transfer near the entrance of the reactor and by kinetics further downstream, when the heat transfer in the autothermal system is efficient. There is not an effective method to reduce channel dimensions if the flow rate remains constant, or to reduce fluid velocities if the residence time is kept constant. The performance of the reactor can be greatly improved by means of proper design of catalyst layer thickness and through adjusting feed composition to minimize or reduce mass transfer limitations in the reactor. Finally, the criteria that can be used to distinguish between different mass transport and kinetics regimes in the reactor with a first-order reforming reaction were presented.

Keywords: Mass transfer limitations; Autothermal systems; Microchannel reactors; Hydrogen production; Steam reforming; Reactor design

Notations

Roman Letters

C	concentration, Equation (14)
C^T	total surface concentration, Equation (27)
D^T	thermal diffusion coefficient, Equation (7)
Da	Damköhler number, Equation (33)
D_{eff}	effective diffusion coefficient, Equation (14)
D_m	molecular diffusion coefficient, Equation (7)
D_K	Knudsen diffusion coefficient, Equation (16)
H	Enthalpy, Equation (23)
K	equilibrium constant, Equation (27)
K_g	number of gaseous species, Equation (5)
K_s	number of surface species, Equation (9)
R	ideal gas constant, Equation (8)
Re	Reynolds number, Equation (30)
Sc	Schmidt number, Equation (30)
Sh	Sherwood number, Equation (30)
T	temperature, Equation (5)
V	diffusion velocity, Equation (6)
W	relative molecular mass, Equation (6)
a	mass transfer coefficient, Equation (30)
b	mass transfer factor, Equation (32)
c	mass transfer factor, Equation (32)
d	mean pore diameter, Equation (17)
d'	characteristic dimension of the channels, Equation (30)
h	enthalpy, Equation (5)
k_R	rate constant for the methanol-steam reforming reaction, Equation (27)
k_W	rate constant for the water-gas shift reaction, Equation (28)
k_D	rate constant for the methanol decomposition reaction, Equation (29)
k_{eff}	effective thermal conductivity, Equation (22)
k_g	thermal conductivity of a gas, Equation (5)
k_s	thermal conductivity of a solid, Equation (10)
l	length of the channels, Equation (31)
m	total number of species, Equation (9)
p	pressure, Equation (2)
p_i	partial pressure of species i, Equation (27)
r_R	rate of the methanol-steam reforming reaction, Equation (27)
r_W	rate of the water-gas shift reaction, Equation (28)
r_D	rate of the methanol decomposition reaction, Equation (29)
$\dot{s}_{i,eff}$	effective rate of appearance of surface species i, Equation (13)
$\dot{s}_m$	rate of appearance of surface species m, Equation (9)
u	fluid velocity, Equation (1)
w	mass fraction, Equation (5)
x, y, z	spatial coordinates, Equation (1)

Greek letters

Γ	density of surface active sites, Equation (9)

Φ	Thiele modulus, Equation (13)
a	ratio between active surface area and geometric surface area, Equation (11)
γ	active surface area per unit volume, Equation (14)
δ	thickness of catalyst layers, Equation (14)
ε_p	porosity, Equation (16)
η	effectiveness factor, Equation (11)
μ	dynamic viscosity, Equation (2)
ρ	density, Equation (1)
θ	surface coverage, Equation (9)
τ_p	tortuosity factor, Equation (16)
ω_k	rate of appearance of gaseous species k, Equation (6)
Superscripts	
*	composite parameter, Equation (27)
b	mass transfer factor, Equation (30)
c	mass transfer factor, Equation (30)
T	total, Equation (27)
(i)	species adsorbed on active site i, Equation (27)
Subscripts	
D	decomposition reaction, Equation (29)
R	reforming reaction, Equation (27)
W	water-gas shift reaction, Equation (28)
1, 1a, 2, 2a	species index, Equation (27)
g	gas, Equation (5)
i	index denoting any chemical species, Equation (13)
k	index denoting any gaseous species, Equation (5)
m	index denoting any surface species, Equation (9)
s	solid, Equation (10)
x, y, z	spatial coordinate components, Equation (1)

1. Introduction

For conventional chemical reactors such as fixed bed reactors, there are various problems in heat and mass transfer processes, which can lead to limitations in the choice of process conditions for steam reforming reactions. The hot spots formed in a fixed bed reactor may significantly reduce the efficiency of the reforming process and the activity of the catalyst [1, 2]. In addition, the strong mass transfer resistance inherent in a fixed bed reactor greatly decrease the rate of the reforming reaction [3, 4]. In microchannel reactors, the ability or tendency to form hot spots is reduced significantly. This reduction is mainly caused by the fact that microchannel reactors can substantially enhance heat transfer capability and permit more precise control of temperatures and residence times [5, 6]. Consequently, it is possible to achieve high levels of conversion and high levels of selectivity to the desired product through the use of microchannel reactors [7, 8].

Reactor design in a chemical process is often directed to approaching isothermal operation of exothermic or endothermic reactions [9, 10]. Approaching isothermal conditions is more readily achieved if microchannel reactors are employed. Even for extremely exothermic or endothermic reactions, microchannel reactor systems can be operated as close as possible to isothermal conditions [11, 12]. This isothermality is of particular usefulness to the kinetics studies on steam reforming reactions with positive reaction enthalpies [13, 14]. When microchannel reactors are designed to perform chemical reaction kinetics studies, it is essential to ensure isothermal conditions and that the concentrations are effectively constant without mass transport limitation to derive intrinsic kinetic parameters [15, 16]. When a microchannel reactor is used for the isothermal operation of heterogeneously catalyzed reactions, the catalyst material is usually coated onto the surface of the reactor wall [17, 18]. Consequently, the reactants must be able to diffuse into the catalyst layer and react on the catalyst surfaces. If the reactants cannot be transferred from the bulk gas phase to the catalyst surface fast enough to keep up with the rate of the reaction occurring in the reactor, the reaction becomes mass transfer controlled [19, 20]. Microchannel reactors are often configured for laminar flow [21, 22], and therefore the rate of mass transfer in a direction perpendicular to the flow direction relies solely on molecular diffusion in the channels.

Knowledge of the mass transport phenomena in microchannel reforming reactors is essential for reactor design and for the optimization of existing reforming processes. Steam reforming reactions are employed in a variety of existing commercial processes [23, 24]. A particularly significant commercial steam reforming process is the methanol steam reforming reaction [25, 26]. Methanol is an important compound with a variety of applications [27, 28]. The primary use of methanol is as a feedstock in the production of various chemicals such as hydrogen [29, 30]. To provide substantially improved reaction kinetics and reactor performance, microchannel methanol-reforming reactors must be configured in a simple and effective manner in which heretofore known problems associated with mass transport phenomena are substantially eliminated [31, 32]. Unfortunately, there is a lack of an accurate understanding of the underlying mass transport phenomena in microchannel methanol-reforming reactors, which is useful to understand and predict the reforming process that occurs on the catalyst surfaces at various operating conditions [33, 34]. It is therefore necessary to determine whether or not a microchannel reforming reactor system is operated in a mass transfer-controlled regime, and provide the necessary criteria so that mass transfer limitations can be effectively eliminated in the reactor.

This study relates to how to minimize or reduce mass transfer limitations in a microchannel methanol-reforming reactor. The reactor was heated using catalytic combustion technology to provide the endothermic heat of reaction needed to reform a mixture of methanol and steam for the production of hydrogen. Numerical simulations were performed using computational fluid dynamics to understand

the mass transport phenomena occurring within the reactor and to develop criteria for determining mass transfer limitations. The effects of catalyst layer thickness, channel characteristic dimension, adding an inert gas, residence time, and fluid velocity on reactor performance were evaluated. The objective of this study is to determine whether or not a microchannel reforming reactor system is operated in a mass transfer-controlled regime, and provide the necessary criteria so that mass transfer limitations can be effectively eliminated in the reactor. Particular focus is placed on the development of the criteria that can be used to distinguish between different mass transport and kinetics regimes in the reactor.

2. Description of the model

Computational fluid dynamics is an effective way to study various transport phenomena in thermally-integrated reforming reactors [35, 36]. In addition, computational fluid dynamics offers great potential for such applications as reactor design [37, 38]. In this study, a three-dimensional computational fluid dynamics model is developed in order to more accurately predict the behavior of an actual microchannel reforming reactor.

2.1. Description of the reactor

The reaction system considered is a thermally-integrated microchannel reactor. A plate type heat exchanger is used as the reactor, which consists of two sets of flow channels. The reactor is used to carry out simultaneous catalytic combustion of methanol and catalytic methanol reforming. The reactor is of compact and simple configuration. The channels are configured for simultaneous passage of the different process reaction streams in a co-current mode. Alternating combustion and reforming channels are in thermal contact with each other. Heat from the combustion channels is used in the steam reforming reaction. Catalysts are coated onto the surfaces of the walls of the channels. The corresponding schematic representation of the computational domain is depicted in Figure 1. Only two half reforming and combustion channels and the surrounding walls are modeled, as depicted schematically in Figure 1, due to the symmetry of the system.

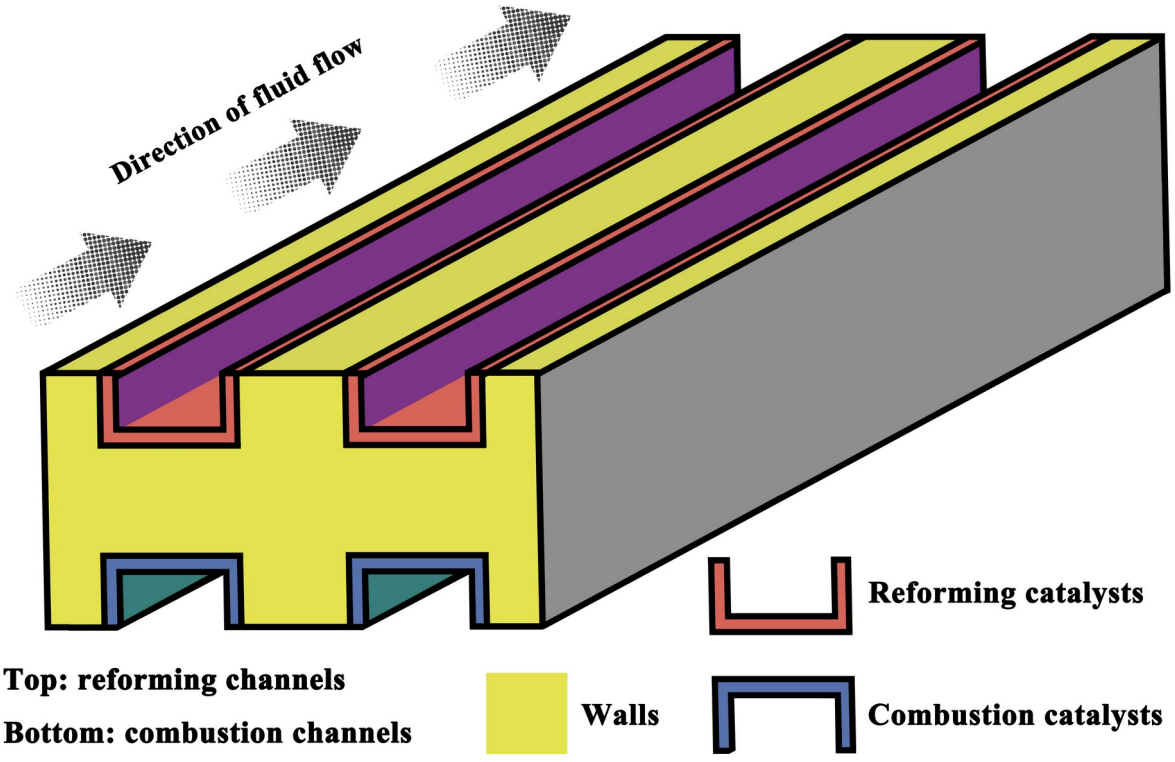

Figure 1. Schematic representation of the computational domain considered in this study. The domain is divided into a plurality of sub-domains such as the regions of fluid, solid, and porous media. The

direction of fluid flow in the channels is indicated by dotted arrows.

Thermochemical processes present the most attractive means for the production of hydrogen. One such process utilizes the reforming reaction of a hydrocarbon fuel, for example, methane [39, 40], with water to produce hydrogen. This process typically requires a significant amount of heat and must be carried out at elevated temperatures to attain the desired level of conversion. For example, the steam methane reforming reaction is strongly endothermic and the process is typically performed under high temperature conditions in order to increase the yield of the desired product [39, 40]. Unfortunately, these high temperatures and heat demands present a multitude of severe challenges for the design and operation of the system. Another such process utilizes the catalytic partial oxidation of a hydrocarbon fuel, for example, methane [41, 42], with oxygen to produce hydrogen. However, the implementation of the process under high temperature conditions is also necessary to enable the catalytic reaction to proceed at short contact times in reduced scale reactors [41, 42]. Another such process, as described here, involves the reaction of an alcohol fuel, for example, methanol [25, 26], with water to produce hydrogen under more moderate conditions. In comparison with methane, methanol permits operation of the system at much lower temperatures and with an insignificant amount of carbon monoxide [25, 26]. This feature offers certain advantages for reactor design and more compact usage, which is especially attractive for commercial applications.

A feed stream comprising methanol and water is introduced into the reactor passing into the reforming channels. The feed stream has a 1:1.4 molar ratio of methanol to water. The reactants are fed to the reactor with a fluid velocity of 2.0 m/s and a temperature of 373 K. Prior to introduction into the reactor, liquid methanol is vaporized and superheated in a vaporizer. The reforming catalyst comprises a mixture of copper and zinc-oxide that are supported on an alumina carrier [43]. Additionally, a feed stream comprising methanol and air is introduced into the reactor passing into the combustion channels, with an equivalence ratio of 0.8. The reactants are fed to the reactor with a velocity of 0.6 m/s and a temperature of 373 K. The combustion catalyst comprises a mixture of copper-oxide and zinc-oxide that are supported on an alumina carrier [44]. The catalysts described above possess good activity, making it possible to operate the autothermal system at relatively low temperatures.

The reactor is 50.0 mm long, and all the combustion channels are designed to have the same dimensions and structures as the reforming channels. The channels may have a variety of cross-sectional shapes, and they are square in cross-section in this study. The distance between the walls is assumed to be 0.7 mm, and thus there is no flame for combustion. The thickness of the dividing walls is also assumed to be 0.7 mm. The catalyst layers in which chemical reactions occur are typically limited in thickness to assure desirable adhesion of the catalyst layers to the dividing walls. In this study, the thickness of the catalyst layers ranges from 0.04 to 0.20 mm. The thermal conductivity of the wall material is 200 W/(m·K) at room temperature. The thermal conductivity of the catalyst supports is 32 W/(m·K) at room temperature. The reactor is operated at a pressure of up to 0.8 MPa.

2.2. Mathematical model

There can be several potential problems associated with computational fluid dynamics modeling of the reactor due to the complexity of the processes involved [45]. The computational complexity of the model is reduced by making simplifying assumptions. The classical continuum approach can be applied, since the collisional mean free path is much lower than the macroscopic length scale of the system. The reactor is operated under steady-state conditions. The ideal gas law is applicable. Laminar flow occurs in the reactor due to the very small Reynolds number, which is defined based on the area-averaged fluid velocity at the flow inlets, obtained in most cases. Both homogeneous reactions and radiative effects are negligible under the conditions specified in this study.

The model includes various mathematical expressions and algorithms for describing fluid

environment and the structure of the reactor, such as the geometry of the reactor, the fluids surrounding the channels in the modeled environment, temperatures, velocities, and boundary conditions defining fluid boundaries. The program ANSYS FLUENT [46], available from ANSYS Inc., Release 18.1, is used to obtain steady-state solutions of the problem.

The continuity equation for each fluid phase can be written as

$$\frac{\partial(\rho u_x)}{\partial x}+\frac{\partial(\rho u_y)}{\partial y}+\frac{\partial(\rho u_z)}{\partial z}=0. \quad (1)$$

The momentum balance for each fluid phase yields

$$-\frac{\partial p}{\partial x}-\frac{\partial}{\partial x}\left[\frac{2}{3}\mu\left(\frac{\partial u_{xx}}{\partial x}+\frac{\partial u_{yx}}{\partial y}+\frac{\partial u_{zx}}{\partial z}\right)\right]+\frac{\partial}{\partial x}\left[\mu\left(\frac{\partial u_x}{\partial x}+\frac{\partial u_x}{\partial x}\right)\right]+\frac{\partial}{\partial y}\left[\mu\left(\frac{\partial u_x}{\partial y}+\frac{\partial u_y}{\partial x}\right)\right]+\frac{\partial}{\partial z}\left[\mu\left(\frac{\partial u_x}{\partial z}+\frac{\partial u_z}{\partial x}\right)\right]=0, \quad (2)$$

$$-\frac{\partial p}{\partial y}-\frac{\partial}{\partial y}\left[\frac{2}{3}\mu\left(\frac{\partial u_{xy}}{\partial x}+\frac{\partial u_{yy}}{\partial y}+\frac{\partial u_{zy}}{\partial z}\right)\right]+\frac{\partial}{\partial x}\left[\mu\left(\frac{\partial u_y}{\partial x}+\frac{\partial u_x}{\partial y}\right)\right]+\frac{\partial}{\partial y}\left[\mu\left(\frac{\partial u_y}{\partial y}+\frac{\partial u_y}{\partial y}\right)\right]+\frac{\partial}{\partial z}\left[\mu\left(\frac{\partial u_y}{\partial z}+\frac{\partial u_z}{\partial y}\right)\right]=0, \quad (3)$$

$$-\frac{\partial p}{\partial z}-\frac{\partial}{\partial z}\left[\frac{2}{3}\mu\left(\frac{\partial u_{xz}}{\partial x}+\frac{\partial u_{yz}}{\partial y}+\frac{\partial u_{zz}}{\partial z}\right)\right]+\frac{\partial}{\partial x}\left[\mu\left(\frac{\partial u_z}{\partial x}+\frac{\partial u_x}{\partial z}\right)\right]+\frac{\partial}{\partial y}\left[\mu\left(\frac{\partial u_z}{\partial y}+\frac{\partial u_y}{\partial z}\right)\right]+\frac{\partial}{\partial z}\left[\mu\left(\frac{\partial u_z}{\partial z}+\frac{\partial u_z}{\partial z}\right)\right]=0. \quad (4)$$

The equation for conservation of energy in each fluid phase can be written as

$$\frac{\partial(\rho u_x h)}{\partial x}+\frac{\partial(\rho u_y h)}{\partial y}+\frac{\partial(\rho u_z h)}{\partial z}+\frac{\partial}{\partial x}\left(\rho\sum_{k=1}^{K_g}w_k h_k V_{k,x}-k_g\frac{\partial T}{\partial x}\right)+\frac{\partial}{\partial y}\left(\rho\sum_{k=1}^{K_g}w_k h_k V_{k,y}-k_g\frac{\partial T}{\partial y}\right)+\frac{\partial}{\partial z}\left(\rho\sum_{k=1}^{K_g}w_k h_k V_{k,z}-k_g\frac{\partial T}{\partial z}\right)=0. \quad (5)$$

The transport of chemical species in each fluid phase is modeled by solving the conservation equation described as follows:

$$\frac{\partial(\rho u_x w_k)}{\partial x}+\frac{\partial(\rho u_y w_k)}{\partial y}+\frac{\partial(\rho u_z w_k)}{\partial z}+\frac{\partial}{\partial x}(\rho w_k V_{k,x})+\frac{\partial}{\partial y}(\rho w_k V_{k,y})+\frac{\partial}{\partial z}(\rho w_k V_{k,z})-\dot{\omega}_k W_k=0, \quad k=1,\ldots,K_g. \quad (6)$$

Multicomponent diffusion is considered in the system, in which the binary molecular diffusion coefficients are determined from the kinetic theory of gases. The full multicomponent diffusion model is computationally expensive. The diffusion velocity of gaseous species k is defined by

$$V_k=-D_{k,m}\nabla\left(\ln\left(w_k\bar{W}W_k^{-1}\right)\right)+\left(D_k^T W\left(\rho w_k\bar{W}\right)^{-1}\right)\nabla(\ln T). \quad (7)$$

The density of a mixture of gases can be determined as

$$p = \rho RT\bar{W}^{-1}. \tag{8}$$

The total number of active surface sites is conserved in each channel as described by

$$\theta_m \dot{s}_m \Gamma^{-1} = 0, \quad m = K_g + 1, \ldots, K_g + K_s. \tag{9}$$

Conservation of energy in the solid phase is described by

$$\frac{\partial}{\partial x}\left(k_s \frac{\partial T}{\partial x} \right) + \frac{\partial}{\partial y}\left(k_s \frac{\partial T}{\partial y} \right) + \frac{\partial}{\partial z}\left(k_s \frac{\partial T}{\partial z} \right) = 0. \tag{10}$$

The mass balance for each gaseous species at the boundaries between the catalyst layers and the fluid phases can be expressed as

$$\eta \alpha W_k (\dot{s}_k)_{boundary} + (\rho w_k V_{k,y})_{boundary} = 0, \quad k = 1, \ldots, K_g, \tag{11}$$

$$\eta \alpha W_k (\dot{s}_k)_{boundary} + (\rho w_k V_{k,z})_{boundary} = 0, \quad k = 1, \ldots, K_g. \tag{12}$$

The catalyst layers are modeled as porous media. When a catalyst layer exceeds a certain critical length, its overall activity, expressed as mass of reactants converted per unit mass of catalyst, begins to diminish [47, 48]. This effect is sometimes expressed as an effectiveness factor [49, 50]. Effectiveness Factor is commonly defined as the rate of reaction in the presence of mass transport limitations divided by the rate of reaction without mass transport limitation

$$\eta = \dot{s}_{i,eff} \dot{s}_i^{-1} = \tanh(\Phi) \Phi^{-1}, \tag{13}$$

where the Thiele modulus can be expressed as

$$\Phi = \delta (\gamma \dot{s}_i)^{0.5} (C_i D_{i,eff})^{-0.5}. \tag{14}$$

The Thiele modulus can be used to predict at what size a catalyst with a defined pore structure and tortuosity and with a known surface activity will become diffusion limited.

The accessible active surface area per unit volume of each catalyst layer can be represented as

$$\gamma = \alpha \delta^{-1}. \tag{15}$$

There are two types of diffusion normally considered [51, 52]. One is bulk or molecular diffusion which occurs when the mean free path between intermolecular collisions is small compared to the mean pore diameter of porous catalyst layers. The other is Knudsen diffusion which occurs when the mean free path is large compared to the mean pore diameter. Transport of reactants and products can occur in the catalyst layers by bulk and Knudsen diffusion. The effective diffusion coefficient of species *i* within the catalyst layers can be expressed as

$$D_{i,eff}^{-1} = \tau_p \varepsilon_p^{-1} \left(D_{i,m}^{-1} + D_{i,k}^{-1} \right). \tag{16}$$

The Knudsen diffusion rate is directly proportional to the mean pore diameter. The Knudsen diffusion coefficient of species *i* is given by

$$D_{i,K} = \frac{d}{3}(8RT)^{0.5}(\pi W_i)^{-0.5} . \quad (17)$$

The balance of energy at the boundaries between the catalyst layers and the fluid phases can be expressed as

$$k_s\left(\frac{\partial T}{\partial y}\right)_{boundary+} - k_g\left(\frac{\partial T}{\partial y}\right)_{boundary-} + \sum_{k=1}^{K_g}(\dot{s}_k h_k W_k)_{boundary} = 0, \quad (18)$$

$$-k_s\left(\frac{\partial T}{\partial y}\right)_{boundary-} + k_g\left(\frac{\partial T}{\partial y}\right)_{boundary+} + \sum_{k=1}^{K_g}(\dot{s}_k h_k W_k)_{boundary} = 0, \quad (19)$$

$$k_s\left(\frac{\partial T}{\partial z}\right)_{boundary+} - k_g\left(\frac{\partial T}{\partial z}\right)_{boundary-} + \sum_{k=1}^{K_g}(\dot{s}_k h_k W_k)_{boundary} = 0, \quad (20)$$

$$-k_s\left(\frac{\partial T}{\partial z}\right)_{boundary-} + k_g\left(\frac{\partial T}{\partial z}\right)_{boundary+} + \sum_{k=1}^{K_g}(\dot{s}_k h_k W_k)_{boundary} = 0. \quad (21)$$

The effective thermal conductivity of the catalyst layers can be described as

$$k_{eff} = \varepsilon_p k_g + (1-\varepsilon_p)k_s . \quad (22)$$

2.3. Chemical kinetic models

The reactor is heated using catalytic combustion technology to provide the endothermic heat of reaction needed to reform a mixture of methanol and steam for the production of hydrogen. The combustion of methanol is conducted catalytically in the reactor and in the absence of flame. This reaction can be written as

$$CH_3OH + 1.5O_2 \Leftrightarrow 2H_2O + CO_2, \ \Delta_r H_m(298.15\ K) = -726.60\ kJ\cdot mol^{-1} . \quad (23)$$

The chemical reactions that occur during reforming include methanol steam reforming and methanol decomposition, which can be expressed, respectively, as

$$CH_3OH + H_2O \Leftrightarrow 3H_2 + CO_2, \ \Delta_r H_m(298.15\ K) = 49.37\ kJ\cdot mol^{-1}, \quad (24)$$

$$CH_3OH \Leftrightarrow 2H_2 + CO, \ \Delta_r H_m(298.15\ K) = 90.47\ kJ\cdot mol^{-1} . \quad (25)$$

Carbon monoxide contained in the hydrogen-rich reformate must be removed, or reduced to an acceptable level in order to allow the use of the product stream in commercial applications. Additional hydrogen can be obtained via the water-gas shift reaction under carefully controlled conditions. This reaction can be written as

$$CO + H_2O \Leftrightarrow H_2 + CO_2, \ \Delta_r H_m(298.15\ K) = -41.10\ kJ\cdot mol^{-1} . \quad (26)$$

The shift reaction is exothermic and reversible, and thus is thermodynamically favored at lower temperatures. This reaction increases hydrogen yield while reducing carbon monoxide.

A detailed description of the physicochemical processes is necessary to accurately predict the essential characteristics of the transport phenomena and exothermic and endothermic reactions occurring within the chemically reacting flow system. More efficient modeling methods, for example, detailed reaction mechanisms, can substantially expand the ability to evaluate critical design tradeoffs for optimizing the system. However, detailed reaction mechanisms require kinetic data, and in

particular, thermodynamic and transport property data with enforced thermodynamic consistency, for the chemical species and elementary reactions involved in the combustion and reforming processes, many of which have not yet been studied experimentally. Theoretical methods for determining the pathways and rates of the elementary reactions involved in the chemical processes have been developed [53, 54], many of which need supercomputer resources to address the issues associated with the quantum mechanical state of the system. Estimation techniques for chemical kinetics and thermodynamic and transport properties required by the detailed reaction mechanisms have also been developed [55, 56], but without experimental data available. In this context, simplified kinetic schemes are included in the model to describe the chemical processes involved in the system.

The contribution of homogeneous reactions is insignificant under the conditions employed in the operation of the reactor [57, 58]. The exothermic process is modeled using a power-law expression developed by Reitz *et al*. [44]. Additionally, the endothermic process is modeled in such a way as to take into account methanol steam reforming and decomposition and the water-gas shift reaction using the kinetic model proposed by Peppley *et al*. [59]. This chemical kinetic model has been extensively validated [60], making the predictions very reliable. The rate of the methanol-steam reforming reaction is expressed by partial pressures

$$r_R = \left[k_R K^*_{CH_3O^{(1)}} \left(p_{CH_3OH} p_{H_2}^{-0.5} \right) \left(1 - k_R^{-1} p_{H_2}^3 p_{CO_2} p_{CH_3OH}^{-1} p_{H_2O}^{-1} \right) C_{S_1}^T C_{S_{1a}}^T \right] \cdot \left[\left(1 + K^*_{CH_3O^{(1)}} \left(p_{CH_3OH} p_{H_2}^{-0.5} \right) + K^*_{HCOO^{(1)}} p_{CO_2} p_{H_2}^{0.5} + K^*_{OH^{(1)}} \left(p_{H_2O} p_{H_2}^{-0.5} \right) \right) \left(1 + K^{0.5}_{H^{(1a)}} p_{H_2}^{0.5} \right) \right]^{-1}. \quad (27)$$

The rate of the water-gas shift reaction is given by

$$r_W = \left[k_W^* K^*_{OH^{(1)}} \left(p_{CO} p_{H_2O} p_{H_2}^{-0.5} \right) \left(1 - k_W^{-1} p_{H_2} p_{CO_2} p_{CO}^{-1} p_{H_2O}^{-1} \right) C_{S_1}^{T^2} \right] \cdot \left[\left(1 + K^*_{CH_3O^{(1)}} \left(p_{CH_3OH} p_{H_2}^{-0.5} \right) + K^*_{HCOO^{(1)}} p_{CO_2} p_{H_2}^{0.5} + K^*_{OH^{(1)}} \left(p_{H_2O} p_{H_2}^{-0.5} \right) \right) \right]^{-2}. \quad (28)$$

The rate of the methanol decomposition reaction described above is given by

$$r_D = \left[k_D K^*_{CH_3O^{(2)}} \left(p_{CH_3OH} p_{H_2}^{-0.5} \right) \left(1 - k_D^{-1} p_{H_2}^2 p_{CO} p_{CH_3OH}^{-1} \right) C_{S_2}^T C_{S_{2a}}^T \right] \cdot \left[\left(1 + K^*_{CH_3O^{(2)}} \left(p_{CH_3OH} p_{H_2}^{-0.5} \right) + K^*_{OH^{(2)}} \left(p_{H_2O} p_{H_2}^{-0.5} \right) \right) \left(1 + K^{0.5}_{H^{(2a)}} p_{H_2}^{0.5} \right) \right]^{-1}. \quad (29)$$

2.4. Numerical methods

The computational fluid dynamics modeling approach used in this study divides the whole computational domain into a plurality of sub-domains such as the regions of fluid, solid, and porous media. More specifically, these sub-domains are discretized into hexahedral elements due to the simplicity of the reactor geometry. The typical mesh employed in this study is non-uniform. In total, the mesh consists of 309,260 nodes.

A mesh independence study is carried out to ensure the independence of the solution. Four meshes are generated with varying level of refinement to verify the mesh independency of the solution. The optimum mesh density is determined to maximize accuracy and minimize computation time. As the mesh density increases, there will be a steady-state converged solution to the problem. The coarsest mesh, consisting of 20,080 nodes in total, is not capable of describing the spatial field features of interest accurately. The solution obtained with a mesh consisting of hundreds of thousands of nodes, for example, 309,260 nodes in total, is cost-effective and reasonably accurate. Higher mesh densities, up to 672,800 nodes in total, do not offer considerable advantages over the density of the mesh used in this study.

Variations in thermodynamic properties with local temperature and local gas composition are

taken into account in the model. Velocity inlet boundary conditions are used to define the flow velocities at flow inlets. Uniform, flat velocity profiles are used at the inlets of the reactor. At the outlets of the reactor, homogeneous Neumann boundary conditions are applied for fluid velocity and temperature. In addition, the no-slip condition is applied at all fluid-solid boundaries.

The three-dimensional computational fluid dynamics solution is deemed to have converged when the residual is less than 10^{-6} for each of the conservation equations described above. The convergence history of the temperature, velocities, and species concentrations is monitored to assure the values level out to the level specified above. The steady state solution process often takes several thousand iterations, the number depending on the size of mesh and the flow characteristics. The numerical simulations performed in this study are rather time-consuming.

2.5. Validation of the model

The cost of model validation is usually quite significant, especially when extremely high model confidence is required. In many cases, there is an existing system that can be captured as part of the model. In this case, the model can be configured to match the characteristics of the existing system and the model outcomes can be compared to outcomes measured from the real system. The is the case with the validation process, since an experimental system similar to the thermally-integrated microchannel reactor described above is currently unavailable with certain features such as methanol fuel, channel dimensions, reactor structure, catalysts, and autothermal operation modes.

The model is valid only if the model is an accurate representation of the actual system [61]. To estimate the accuracy of the model, the results predicted by the model are compared with the experimental data available in the literature [62]. Steam reforming of methanol is performed in a microchannel reactor under different temperature conditions. The channels of the reactor are rectangular in cross-section, and they are 0.6 mm in total height, 33.0 mm in length, and 0.5 mm in width. The reactor is made of stainless-steel plates. The reforming reaction is conducted at temperatures ranging from 473 to 533 K. The heat required by the endothermic process is supplied directly by an electrical heating device. The feed stream has a 1:1.1 molar ratio of methanol to water. The feed gas mixture is introduced into the reactor at a temperature of 393 K. The reforming catalyst used in the experiments is the same as that described previously, but their catalytic activities may differ significantly from each other. Accordingly, some of the kinetic parameters, for example, the rate constants described above, are determined by globally fitting the predetermined kinetic model for the reforming reaction. Numerical simulations are conducted for the reactor operating under the same set of reaction conditions used in the experiments by utilizing the model described above. It is worth noting that the exact same operating conditions and design parameters as those employed in the experiments are used in the simulation. The results are presented in Figure 2, in which methanol conversion and hydrogen production rate versus reaction temperature are plotted for the reactor. The results obtained from the model are in satisfactory agreement with the data measured from the reactor.

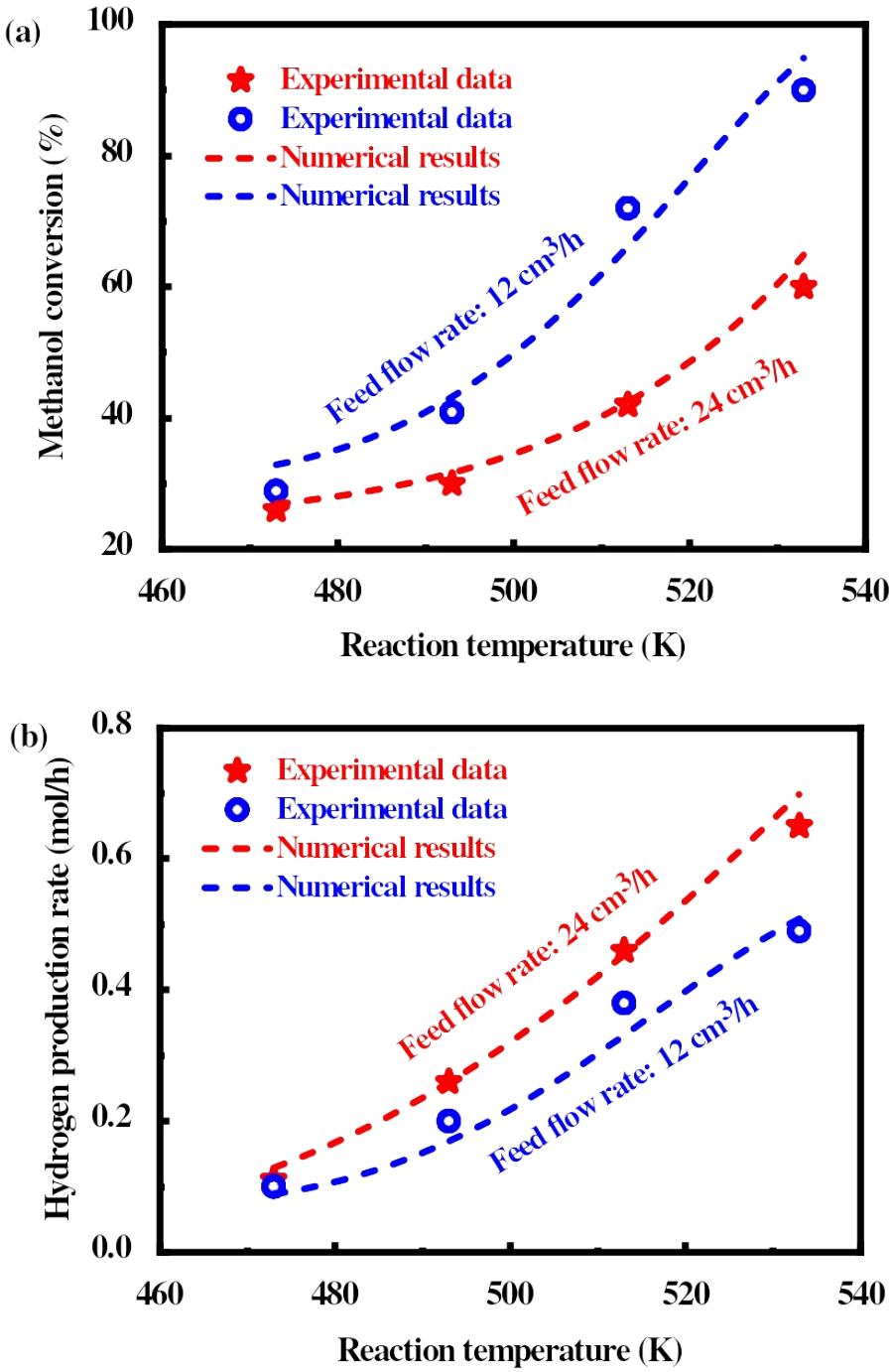

Figure 2. (a) Methanol conversion and (b) hydrogen production rate as a function of reaction temperature. The experimental data are included for comparison.

The model should be validated to the degree required for the model's intended purpose or application. There is no significant difference between the experimental conditions and the design parameters used in this study. The model within its domain of applicability possesses a satisfactory range of accuracy consistent with the intended application of the model, as discussed above. To obtain a higher degree of confidence in the model and its results, however, comparisons of the model's and real system's output behaviors for several different sets of experimental conditions are usually required. Further validation is needed to ensure that the model's output behavior has the accuracy required for the model's intended purpose over the domain of the model's intended applicability.

3. Results and discussion

3.1. Operation regimes

Preferably, the system can be maintained adiabatic and isothermal in order to determine the operation regimes for the methanol-steam reforming reaction in the reactor. The reactor should be configured to enhance desired thermal and mass transfer characteristics for the system. Efficient heat transfer processes make possible decreased mass transfer limitations in the endothermic reforming channels. Contour plots of temperature, species concentrations, enthalpy, and sensible enthalpy are presented in Figure 3 for the reactor. The thermal conductivity of the wall material is very high so that heat can be transferred by indirect heat exchange between the two process reaction streams at a rate sufficient to maintain the reactor at substantially isothermal conditions. The difference between the highest and lowest temperature within the dividing walls is no greater than 10 K, as presented by the temperature contour plot in Figure 3. This results in efficient heat transfer in the reactor, as presented by the enthalpy and sensible enthalpy contour plots in Figure 3. The term "isothermal" as used herein means substantially uniform temperature. It is therefore possible to achieve substantially isothermal operation of the system. One design consideration for approaching isothermal conditions in the reactor is relatively small dimensions for the channels. This provides a relatively small resistance to heat transfer relative to the heat generated per unit volume of reaction space within the channels. Another such design consideration is a relatively long length for the channels, which reduces the heat release per unit volume of reaction within the channels and also promotes isothermality.

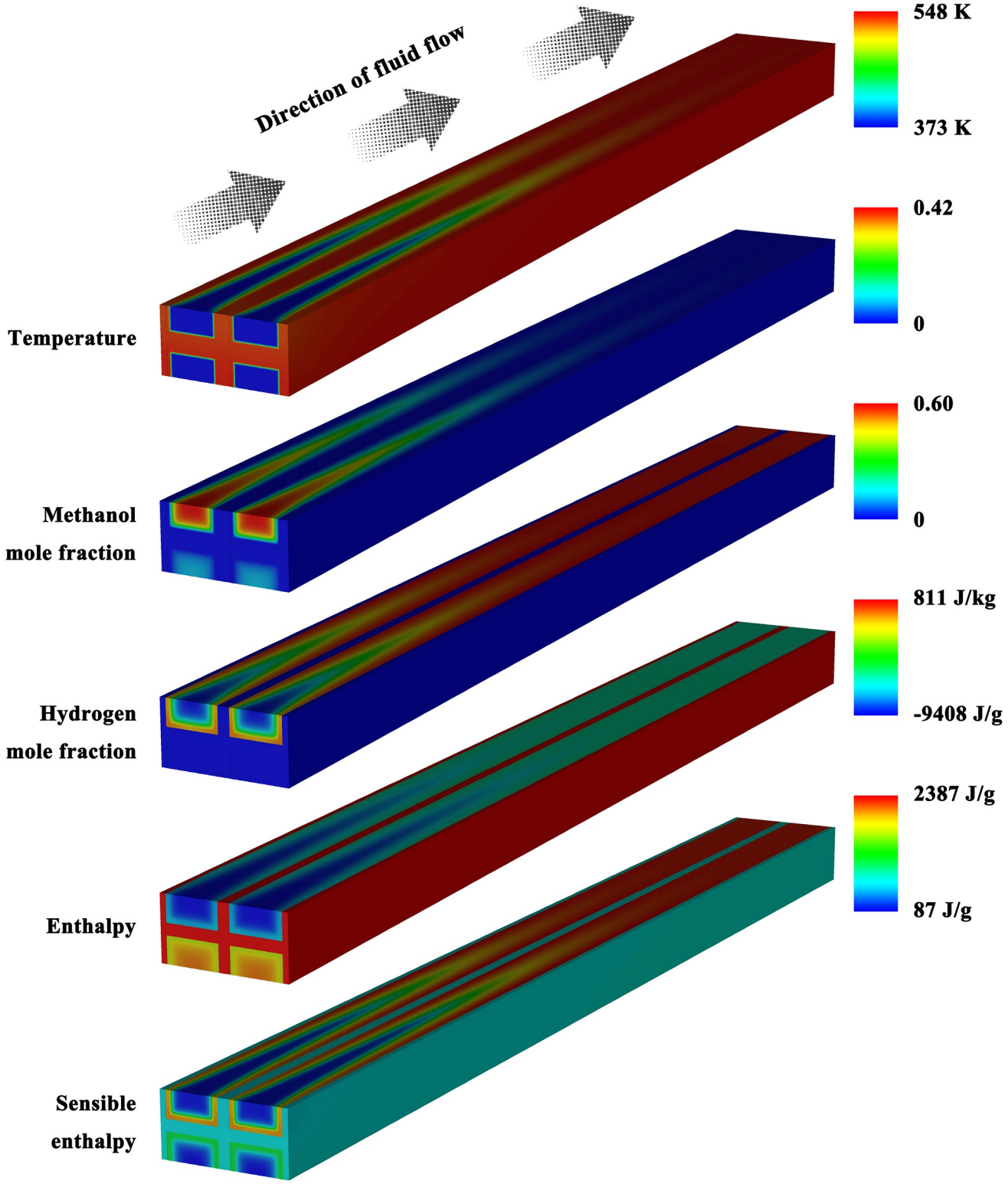

Figure 3. Contour plots of temperature, species concentrations, enthalpy, and sensible enthalpy for the reactor. The distance between the walls is 0.7 mm. The thickness of the catalyst layers is 0.1 mm. The fluid velocity at the flow inlets of the reforming channels is 2.0 m/s, and the fluid velocity at the flow inlets of the combustion channels is 0.6 m/s. The thermal conductivity of the wall material is 200 W/(m·K) at room temperature.

Near the entrance of the reactor, the system is subjected to steep concentration gradients, and thus the limiting factor controlling the rate of the reforming reaction is the rate of mass transfer. Therefore, the rate of the reforming reaction is limited by mass transfer near the entrance of the reactor, despite the small characteristic length scale of the system. Further downstream, the rate of the reforming reaction is

limited by kinetics, since there are no significant concentration gradients within the channels, as presented by the concentration contour plots in Figure 3. Overall, the rate of the reforming reaction is limited by mass transfer near the entrance of the reactor, and by kinetics further downstream. This will be discussed in more detail later.

The reforming reaction is carried out in the reactor configured and operated in a manner such that the conversion of methanol is highest and the selectivity to the desired product is maximized. It is therefore necessary to determine whether or not the reaction system is operated in a mass transfer-controlled regime, and provide the necessary criteria so that the mass transfer within the microchannel reactor can be effective. The Damköhler number can be used to relate the reforming reaction timescale to the mass transfer rate for the chemically reacting flow system. Assuming the reforming reaction to be first order, the system is operated in a mass transfer-controlled regime when the following criterion is satisfied [63, 64]

$$\mathrm{Da} = k_R d' D_m^{-1} > 100 \quad (33)$$

In this case, the rate of the reforming reaction is sufficiently fast that methanol is reacted almost immediately upon reaching the surface of the catalyst. Under mass transfer limited conditions, the net rate of the reforming reaction is not controlled by the catalyst activity or a fuel's reactivity, and is therefore independent of fuel type.

The system is operated in a kinetically-controlled regime and is essentially free of mass transfer limitations when the following criterion is satisfied [63, 64]

$$\mathrm{Da} = k_R d' D_m^{-1} < 0.1 \quad (34)$$

There is a transition from a kinetically-controlled regime to a mass transfer-controlled regime when the Damköhler number varies in the following range [63, 64]

$$0.1 \leq \mathrm{Da} = k_R d' D_m^{-1} \leq 100 \quad (35)$$

The results obtained for different channel characteristic dimensions are presented in Figure 4, in which the operation regimes, determined by the Damköhler number, for the methanol-steam reforming reaction in the reactor are presented. The residence time of the reforming reaction mixture passing through the reactor varies depending upon the characteristic dimension of the channels. As the characteristic dimension decreases, there is a transition from a mass transfer-controlled regime to a transient regime and then to a kinetically-controlled regime, with net reaction rate ultimately limited by reaction rate in the catalyst layers. Large characteristic dimensions of the channels increase resistance to mass transfer within the reactor during the reforming reaction. Such mass transfer resistance can prevent the reactants from reaching the catalyst layers as fast as they can react and thereby can result in inefficient utilization of the reforming catalyst. Therefore, due to such limitations on the mass transfer within the reactor, the potential for the effectiveness of the catalysts appears to be limited. To minimize mass transfer resistances, the channels should be as small as possible. Diffusion limitations can be eliminated by reducing the characteristic dimensions of the channels. Small characteristic dimensions of the channels make possible a reduction in mass transfer limitations, thereby improving the performance of the reactor. Therefore, the reforming reaction may advantageously be carried out in small channels. However, small channels cause disadvantageously high pressure drops. In the present case, the system is operated in a kinetically-controlled regime and is therefore essentially free of mass transfer limitations at the specified operating conditions.

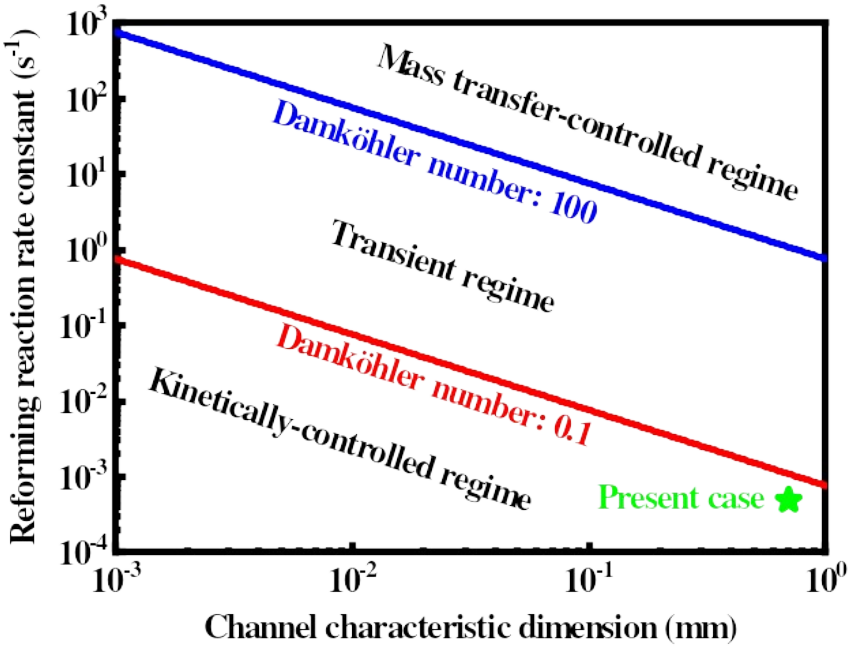

Figure 4. Map of operation regimes for the methanol-steam reforming reaction in the reactor determined by the Damköhler number. The results obtained for the present case are indicated by a five-pointed star. The thickness of the catalyst layers is 0.1 mm. The fluid velocity at the flow inlets of the reforming channels is 2.0 m/s, and the fluid velocity at the flow inlets of the combustion channels is 0.6 m/s.

Species concentration profiles in the transverse direction can also be used to determine what regime the system is operated [65, 66]. The system is operated in a mass transfer-controlled regime when reactant concentrations are low in the vicinity of the catalyst layers. On the other hand, the system is operated in a kinetically-controlled regime when reactant concentrations are high in the vicinity of the catalyst layers. Contour plots of methanol and hydrogen concentrations in the plane perpendicular to the streamwise direction are presented in Figure 5 for different streamwise distances. The system is subjected to steep gradients of methanol and hydrogen concentrations near the entrance of the reactor, whereas there are no significant concentration gradients within the channels further downstream. When compared to the corresponding bulk concentration in the reforming channels, methanol concentrations in the vicinity of the catalyst layers are low near the entrance of the reactor and high further downstream. Therefore, the rate of the reforming reaction is limited by mass transfer near the entrance of the reactor, and by kinetics further downstream, as discussed above. On the other hand, the desired product is efficiently removed from the vicinity of the catalyst layers. The continuous removal of the desired product may substantially eliminate mass transport limitations in diffusion inhibited systems and would greatly increase overall reaction rate and product yield.

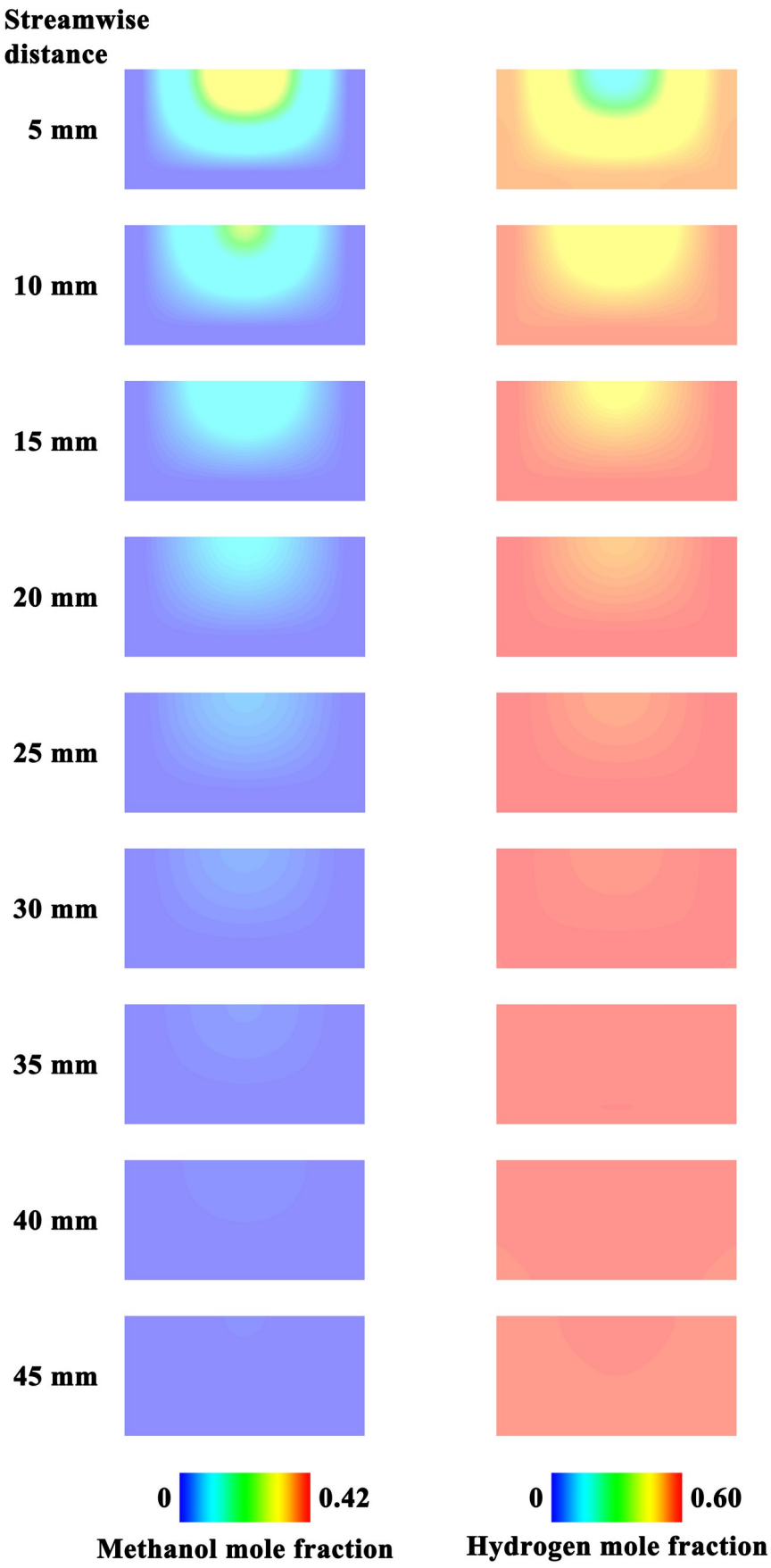

Figure 5. Contour plots of methanol and hydrogen concentrations in the plane perpendicular to the streamwise direction on a two-dimensional format. The distance between the walls is 0.7 mm. The thickness of the catalyst layers is 0.1 mm. The fluid velocity at the flow inlets of the reforming channels is 2.0 m/s, and the fluid velocity at the flow inlets of the combustion channels is 0.6 m/s.

To determine the operation regimes for the methanol-steam reforming reaction in the reactor, two boundary limits are defined here in terms of the ratio between the concentration of one or more reactants in the vicinity of the catalyst layers and the corresponding average concentration for the cross section of the flow channel. In this study, the lower limit of the dimensionless reactant concentration ratio is assumed to be 0.05 [65, 66], and the upper limit of the dimensionless reactant concentration ratio is assumed to be 0.95 [67, 68]. The results obtained for different reforming reaction rates are presented in Figure 6, in which the dimensionless methanol concentration ratio is expressed as a function of the rate of the reforming reaction, and the operation regimes, determined by the dimensionless methanol concentration ratio, for the methanol-steam reforming reaction in the reactor are also presented. If the dimensionless methanol concentration ratio reaches the lower limit defined above, it can be assumed that the system is operated in a mass transfer-controlled regime. In contrast, the reforming reaction becomes kinetically-controlled when the dimensionless methanol concentration ratio reaches the upper limit defined above. Near the entrance of the reactor, the rate of the reforming reaction is high, and the reforming reaction is mass transfer controlled. Further downstream, the rate of the reforming reaction is low, and the reforming reaction becomes kinetically-controlled. Overall, the rate of the reforming reaction is limited by mass transfer near the entrance of the reactor, and by kinetics further downstream, as discussed above.

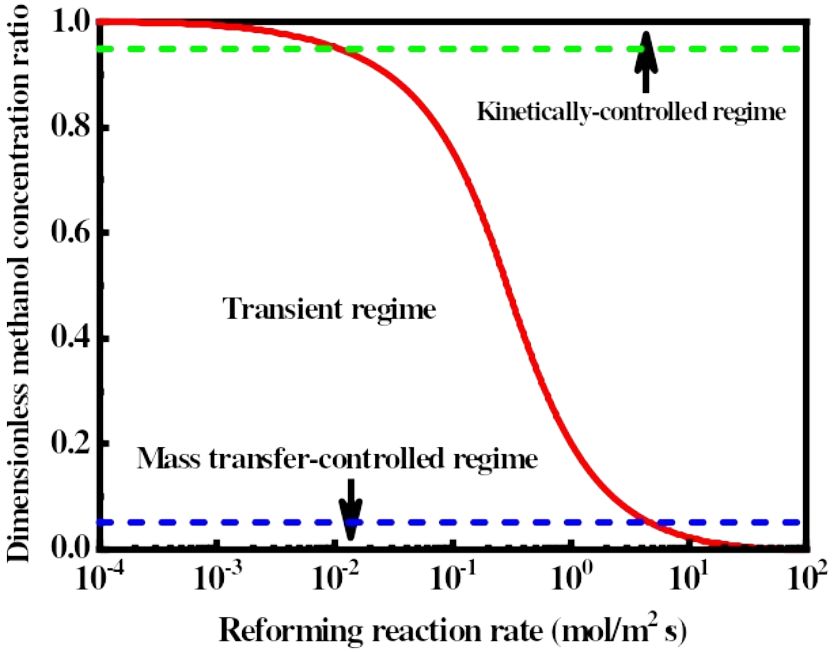

Figure 6. Map of operation regimes for the methanol-steam reforming reaction in the reactor determined by the dimensionless methanol concentration ratio. The thickness of the catalyst layers is 0.1 mm. The fluid velocity at the flow inlets of the reforming channels is 2.0 m/s, and the fluid velocity at the flow inlets of the combustion channels is 0.6 m/s.

3.2. Effect of fluid velocity

The thickness of the mass transport boundary layers formed within the channels can be reduced by utilizing high fluid velocities to enhance the mass transfer within the reactor. The effect of fluid velocity on methanol conversion is investigated. The results are presented in Figure 7, in which methanol conversion is expressed as a function of the residence time of the reforming reaction mixture passing through the reactor. For different fluid velocities at the flow inlets of the reforming channels, the residence time is kept constant by reducing the length of the reactor. The residence time play an important role in the performance of the reactor. Methanol conversion increases with increasing the residence time. However, fluid velocities have little effect on methanol conversion if the residence time

is kept constant. High fluid velocities are not necessarily a high degree of methanol conversion, although there is a reduction in the thickness of boundary layers and thus an enhancement in mass transfer within the reactor. The Sherwood number is a dimensionless number used in mass-transfer operation. In the case of laminar flow in the channels, the Sherwood number can also be further defined using dimensional analysis as follows [69, 70]:

$$\mathrm{Sh} = a\,\mathrm{Re}^{b}\,\mathrm{Sc}^{c} = a\left(\rho u_x d'\mu^{-1}\right)^{b}\left(\mu\rho^{-1}D_m^{-1}\right)^{c}. \tag{30}$$

The Sherwood number can be expressed using the heat-mass transfer analogy as follows [71, 72]:

$$\mathrm{Sh} = a, \quad \text{small } \mathrm{ReSc}d'l^{-1}, \tag{31}$$

$$\mathrm{Sh} = b\left(\mathrm{ReSc}d'l^{-1}\right)^{\frac{1}{3}} = b\left(\mathrm{Sc}\rho d'^{2}\mu^{-1}u_x l^{-1}\right)^{\frac{1}{3}}, \quad \text{large } \mathrm{ReSc}d'l^{-1}. \tag{32}$$

In the case of laminar flow in the channels, the rate of mass transfer within the continuous flow reactor depends upon the residence time of the reforming reaction mixture passing through the reactor, as expressed by the heat-mass transfer analogy defined above. If the residence time remains constant, high fluid velocities have no significant effect on the rate of mass transfer within the reactor.

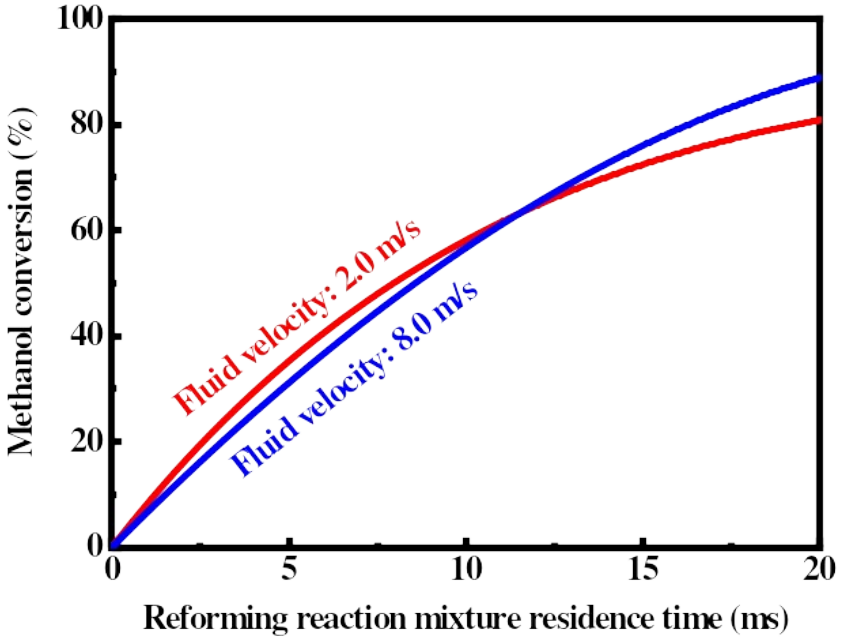

Figure 7. Methanol conversion as a function of the residence time of the reforming reaction mixture passing through the reactor. The distance between the walls is 0.7 mm. The thickness of the catalyst layers is 0.1 mm. The fluid velocity at the flow inlets of the reforming channels is 2.0 and 8.0 m/s, respectively. For different fluid velocities at the flow inlets of the reforming channels, the residence time is kept constant by reducing the length of the reactor.

3.3. Effect of adding an inert gas

The presence of an inert gas in a feed gas mixture can affect the fluid transport properties such as thermal and mass diffusion coefficients. The change of thermal diffusion coefficients may have a significant effect on the rate of heat transfer within the autothermal system [73, 74]. In addition, the change of thermal diffusion coefficients will cause heavy molecules to diffuse less rapidly, and light molecules to diffuse more rapidly, towards catalytic surfaces due to the Soret effect. On the other hand, the mass diffusion coefficient for a chemical species in the mixture is dependent upon the mixture composition [73, 74]. The presence of an inert gas can cause changes in the molecular diffusion

coefficients of the gaseous species involved in the multi-component system. Since the heat and mass transport processes can be significant within the system, the mass transfer limitations in the reactor may be reduced by adding an inert gas with high molecular diffusion coefficients in the feed gas mixtures, thereby enhancing the effective reforming reaction rate. Therefore, the effect of adding an inert gas in the feed gas mixtures on the performance of the reactor is investigated in order to better understand the mass transport phenomena occurring within the reactor.

Numerical simulations are performed in the case that an inert gas such as argon and helium is added into the feed stream. The inert gas is present in each of the feed gas mixtures in a concentration of 20 volume percent. The total gas pressure remains constant. The results are presented in Figure 8, in which methanol conversion is expressed as a function of the maximum rate of the reforming reaction. When the maximum rate of the reforming reaction is low, methanol conversion is identical and very low, irrespective of feed composition. In this case, the reforming reaction is kinetically controlled, and is essentially free of mass transfer limitations. When the maximum rate of the reforming reaction is high, there is an increase in methanol conversion. The effect of adding an inert gas becomes more pronounced with increasing the maximum rate of the reforming reaction. This effect is due to the change of the molecular diffusion coefficient of the gaseous species involved in the system. The inert gases described above can increase molecular diffusion coefficients and thus enhance the mass transfer within the reactor, which eventually leads to an increase in methanol conversion. When the maximum rate of the reforming reaction is very high, the kinetics of the reforming reaction has little effect on the methanol conversion within the reactor. In this case, the methanol conversion levels off regardless of a further increase in the rate of the reforming reaction. The reforming reaction is fully controlled by mass transfer, which is determined by the molecular diffusion coefficient of the gaseous species involved in the system. There is considerable difference in the methanol conversion obtained with argon and helium, since the rates of diffusion of the inert gases in their respective reaction mixtures differ from each other. On the other hand, the diffusion coefficient for a binary mixture of gases is dependent upon the total pressure. The mass transfer within the reactor can be enhanced by reducing the total gas pressure while keeping substantially constant the partial pressure of the reactants, without affecting the kinetics of the reforming reaction. Therefore, the mass transfer within the reactor can be further enhanced by using this method, thereby facilitating the reforming reaction.

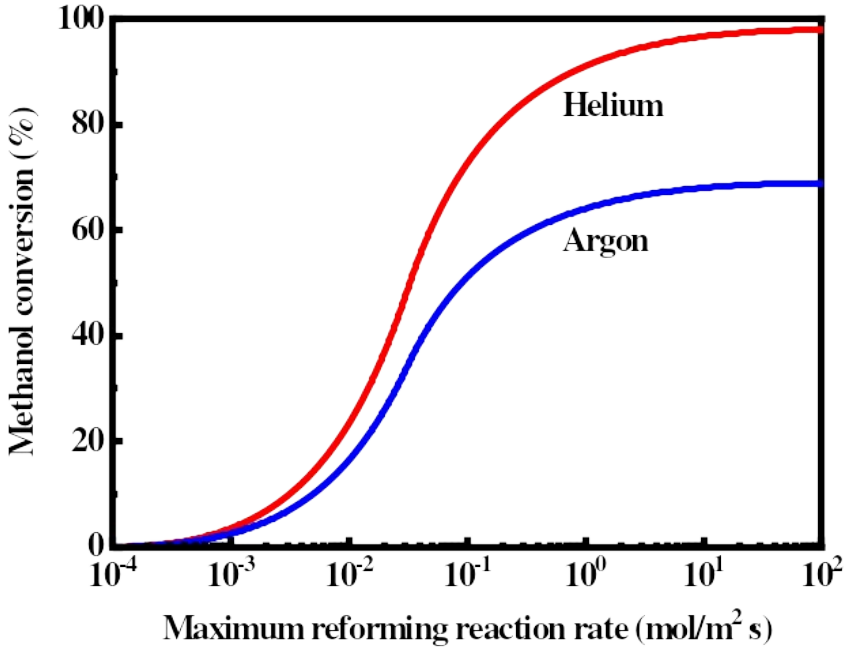

Figure 8. Effect of adding an inert gas on the methanol conversion in the reforming channels for different maximum rates of the reforming reaction. The total gas pressure remains constant. The

distance between the walls is 0.7 mm. The thickness of the catalyst layers is 0.1 mm. The fluid velocity at the flow inlets of the reforming channels is 2.0 m/s, and the fluid velocity at the flow inlets of the combustion channels is 0.6 m/s.

3.4. Effect of channel characteristic dimension

The results obtained for different channel characteristic dimensions are compared at the same reaction conditions. The flow rates of the reaction mixtures flowing in the channels are adjusted in such a manner as to maintain a substantially constant flow velocity of each reaction mixture passing through the reactor over the range of channel characteristic dimensions. More specifically, the flow rate of the methanol and water mixture flowing in the reforming channels is adjusted so that the flow velocity of the reforming reaction mixture passing through the reactor remains about constant over a wide range of channel characteristic dimensions. Such adjustment is also performed for the flow rate of the methanol and air mixture flowing in the combustion channels. Accordingly, the residence time of each reaction mixture passing through the reactor is kept almost constant. The results are presented in Figure 9, in which methanol conversion and hydrogen yield are expressed as a function of the characteristic dimension of the channels. The Reynolds number of the system can be used to indicate whether flow in the channels may be laminar or turbulent. Specifically, the Reynolds number can be used to predict flow patterns in the channels, and laminar flow occurs at low Reynolds numbers. The velocity, density, and viscosity of the fluid will tend to vary widely in the reforming channels or in the combustion channels. In the system, however, the Reynolds number associated with the maximum channel characteristic dimension is less than 800, which is well within the laminar flow regime.

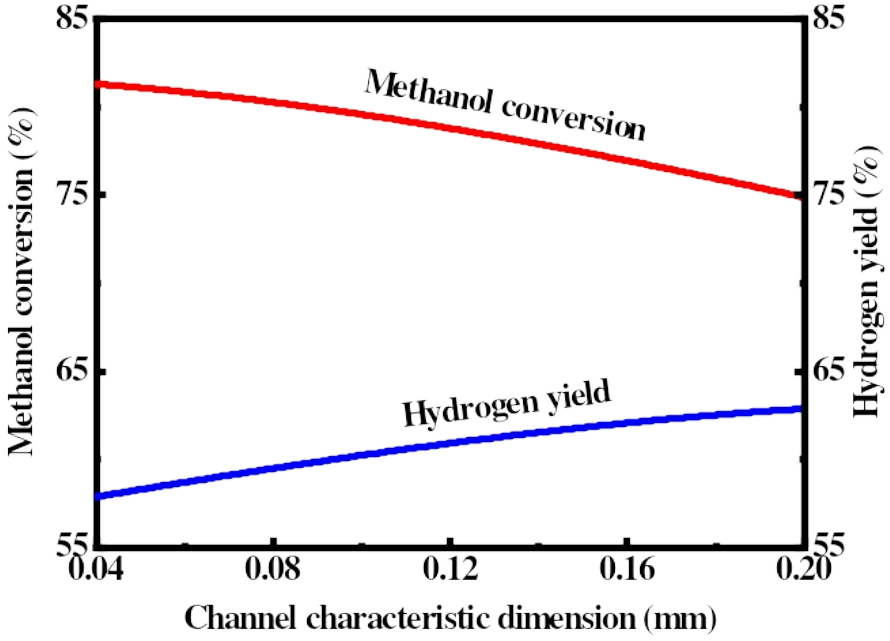

Figure 9. Effect of channel characteristic dimension on the methanol conversion and hydrogen yield in the reforming channels. The thickness of the catalyst layers is 0.1 mm. When the distance between the walls is 0.7 mm, the fluid velocity at the flow inlets of the reforming channels is 2.0 m/s, and the fluid velocity at the flow inlets of the combustion channels is 0.6 m/s. The flow rates of the reaction mixtures flowing in the channels are adjusted in such a manner as to maintain a substantially constant flow velocity of each reaction mixture passing through the reactor over the range of channel characteristic dimensions. Accordingly, the residence time of each reaction mixture passing through the reactor is kept almost constant.

If the reactor is operated in a mass transfer limited region in which the rate of the reforming reaction is limited by mass transfer, fuel conversion and product yield will increase with decreasing the

characteristic dimension of the channels. However, there is no significant difference in both fuel conversion and product yield between different channel characteristic dimensions, as indicated by the results presented in Figure 9. More specifically, as the characteristic dimension of the channels increases while maintaining substantially constant residence time, the methanol conversion in the reforming channels decreases slightly but the hydrogen yield obtained from the reforming reaction increases slightly due to the increased flow rates of the reaction mixtures flowing in the channels. Overall, the characteristic dimension of the channels has little effect on the performance of the reactor under the specified conditions. Therefore, the rate of external mass transfer increases to such an extent that the reactants can be transferred in the gas phase fast enough to keep up with the rate of the reforming reaction, the reforming reaction do not shift to mass transfer control, and the rate of the reforming reaction levels off regardless of further channel characteristic dimension decreases. In this case, the rate of the reforming reaction is no longer limited by external mass transfer at the specified operating conditions, making it possible to operate the system without diffusion limitations. The rate of the reforming reaction is substantially increased beyond the external mass transfer limitation, and such a high reaction rate permits high fluid velocities in the channels.

3.5. Effect of catalyst layer thickness

The allowable thickness of catalyst layers is a critical parameter in the performance of a microchemical system [75, 76]. The effect of catalyst layer thickness is investigated for a given set of reaction conditions. The thickness of the catalyst layers varies between 0.04 and 0.20 mm. The results are presented in Figure 10, in which methanol conversion is expressed as a function of the thickness of the catalyst layers. Additionally, the rate of the reforming reaction is determined with the model described above, when the thickness of the catalyst layers is equal to 0.04, 0.12, and 0.20 mm, respectively. The results are obtained at a streamwise distance of 20.0 mm. The methanol conversion in the reactor increases with increasing catalyst layer thickness. More specifically, in relatively thin catalyst layers, the methanol conversion increases rapidly with catalyst layer thickness. As the catalyst layer thickness is increased further, the methanol conversion enters a transition region wherein the rate of intraphase mass transport within the catalyst layers begins to limit the further increase of methanol conversion. As the catalyst layer thickness is increased still further, the rate of the reforming reaction enters a mass transfer limited region wherein the reactants cannot be transferred into the catalyst layers fast enough to keep up with the reforming reaction occurring within the catalyst layers, and the methanol conversion levels off regardless of a further increase in the thickness of the catalyst layers. In the extreme case that the catalyst layers are very thick, the rate of the reforming reaction can be close to zero in the interiors of the catalyst layers. There will eventually be significant limitations of internal mass transfer within the reactor. In the mass transfer limited region, higher activity of the reforming catalyst does not lead to an increase in the rate of the reforming reaction [77, 78]. The only apparent method is to increase the rate of mass transfer within the reactor. This method can be effective, since the resistance to mass transfer within the catalyst layers depends on catalyst layer properties such as porosity, pore size, and surface active site density. Therefore, a larger amount of hydrogen can be produced by optimizing the properties of the catalyst layers.

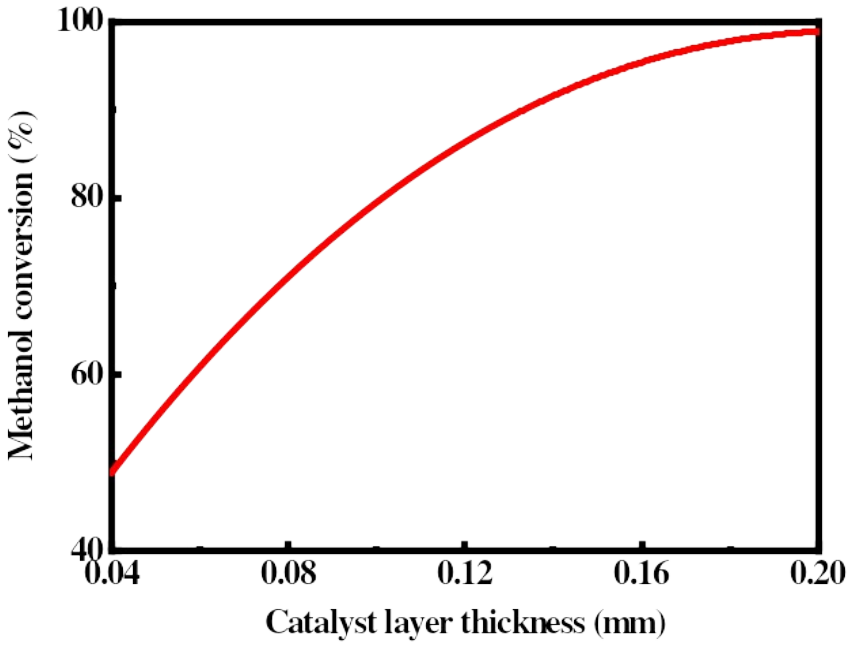

Figure 10. Methanol conversion as a function of the thickness of the catalyst layers. The amount of the catalysts employed varies depending upon the thickness of catalyst layers. The distance between the walls is 0.7 mm. The fluid velocity at the flow inlets of the reforming channels is 2.0 m/s, and the fluid velocity at the flow inlets of the combustion channels is 0.6 m/s.

4. Conclusions

This study was focused mainly upon the essential characteristics of mass transfer processes in a microchannel reforming reactor. The reactor was designed for thermochemically producing hydrogen. Numerical simulations were performed using computational fluid dynamics to better understand the mass transport phenomena occurring within the reactor. Of particular concern were those conditions where the methanol reforming reaction is mass transfer-controlled. The criteria that can be used to distinguish between different mass transport and kinetics regimes in the reactor were developed.

- When the heat transfer in the thermally integrated system is efficient, the rate of the methanol reforming reaction is limited by mass transport near the entrance of the reactor and by chemical kinetics further downstream.
- The mass transfer limitations in the reactor can be reduced by optimizing the thickness of catalyst layers and through adjusting feed composition, whereby the performance of the reactor can be substantially improved.
- Fluid velocities have little effect on the mass transfer limitations in the reactor, if the residence time of the reforming reaction mixture passing through the reactor is kept constant.
- The mass transfer limitations in the reactor can be effectively eliminated by reducing the characteristic dimensions of the channels. However, this is not an effective method, if the flow rate of the reforming reaction mixture passing through the reactor remains constant.
- A long residence time of the reforming reaction mixture passing through the reactor reduces the mass transfer limitations, thereby allowing the reforming reaction to more closely approach the intrinsic kinetic rate.
- The mass transfer limitations in the reactor can be effectively reduced by adding an inert gas with high molecular diffusion coefficients in each of the feed gas mixtures, thereby enhancing the effective rate of the reforming reaction, with improved reactor performance and an increase in methanol conversion.

References

[1] H.G. Düsterwald, B. Höhlein, H. Kraut, J. Meusinger, R. Peters, and U. Stimming. Methanol steam-reforming in a catalytic fixed bed reactor. *Chemical Engineering & Technology*, Volume 20, Issue 9, 1997, Pages 617-623.

[2] R. Tesser, M. Di Serio, and E. Santacesaria. Methanol steam reforming: A comparison of different kinetics in the simulation of a packed bed reactor. *Chemical Engineering Journal*, Volume 154, Issues 1-3, 2009, Pages 69-75.

[3] D.A. Hickman, J.C. Degenstein, and F.H. Ribeiro. Fundamental principles of laboratory fixed bed reactor design. *Current Opinion in Chemical Engineering*, Volume 13, 2016, Pages 1-9.

[4] G. Kolios, J. Frauhammer, and G. Eigenberger. Autothermal fixed-bed reactor concepts. *Chemical Engineering Science*, Volume 55, Issue 24, 2000, Pages 5945-5967.

[5] A. Kundu, J.M. Park, J.E. Ahn, S.S. Park, Y.G. Shul, and H.S. Han. Micro-channel reactor for steam reforming of methanol. *Fuel*, Volume 86, Issue 9, 2007, Pages 1331-1336.

[6] J. Na, K.S. Kshetrimayum, I. Jung, S. Park, Y. Lee, O. Kwon, Y. Mo, J. Chung, J. Yi, U. Lee, and C. Han. Optimal design and operation of Fischer-Tropsch microchannel reactor for pilot-scale compact Gas-to-Liquid process. *Chemical Engineering and Processing - Process Intensification*, Volume 128, 2018, Pages 63-76.

[7] N. Al-Rifai, E. Cao, V. Dua, and A. Gavriilidis. Microreaction technology aided catalytic process design. *Current Opinion in Chemical Engineering*, Volume 2, Issue 3, 2013, Pages 338-345.

[8] A. Tonkovich, D. Kuhlmann, A. Rogers, J. McDaniel, S. Fitzgerald, R. Arora, and T. Yuschak. Microchannel technology scale-up to commercial capacity. *Chemical Engineering Research and Design*, Volume 83, Issue 6, 2005, Pages 634-639.

[9] J.M. Commenge, L. Falk, J.P. Corriou, and M. Matlosz. Optimal design for flow uniformity in microchannel reactors. *AIChE Journal*, Volume 48, Issue 2, 2002, Pages 345-358.

[10] S. Walter, S. Malmberg, B. Schmidt, and M.A. Liauw. Comparison of microchannel and fixed bed reactors for selective oxidation reactions: Isoprene to citraconic anhydride. *Chemical Engineering Research and Design*, Volume 83, Issue 8, 2005, Pages 1019-1029.

[11] I. Rossetti. Continuous flow (micro-)reactors for heterogeneously catalyzed reactions: Main design and modelling issues. *Catalysis Today*, Volume 308, 2018, Pages 20-31.

[12] P. Pfeifer, K. Schubert, M.A. Liauw, and G. Emig. Electrically heated microreactors for methanol steam reforming. *Chemical Engineering Research and Design*, Volume 81, Issue 7, 2003, Pages 711-720.

[13] R.O. Idem and N.N. Bakhshi. Production of hydrogen from methanol. 2. Experimental studies. *Industrial & Engineering Chemistry Research*, Volume 33, Issue 9, 1994, Pages 2056-2065.

[14] R.O. Idem and N.N. Bakhshi. Kinetic modeling of the production of hydrogen from the methanol-steam reforming process over Mn-promoted coprecipitated Cu-Al catalyst. *Chemical Engineering Science*, Volume 51, Issue 14, 1996, Pages 3697-3708.

[15] G.G. Hammes. Introduction of hydrogen routines. *Principles of Chemical Kinetics*, Academic Press, Inc., New York, the United States, 1978, ISBN: 978-0-12-321950-3.

[16] A.K. Coker and C.A. Kayode. *Modeling of Chemical Kinetics and Reactor Design*, Elsevier Inc., Oxford, the United Kingdom, 2001, ISBN: 978-0-88415-481-5.

[17] G. Liesche and K. Sundmacher. Productivity versus product quality: Exploring the limits of autothermal microchannel reactors in methane steam reforming. *Chemical Engineering Journal*, Volume 377, 2019, Article Number: 120048.

[18] Y.-X. Huang, J.-Y. Jang, and C.-H. Cheng. Fractal channel design in a micro methanol steam reformer. *International Journal of Hydrogen Energy*, Volume 39, Issue 5, 2014, Pages 1998-2007.

[19] V. Balakotaiah and D.H. West. Shape normalization and analysis of the mass transfer controlled regime in catalytic monoliths. *Chemical Engineering Science*, Volume 57, Issue 8, 2002, Pages 1269-1286.

[20] D.H. West, V. Balakotaiah, and Z. Jovanovic. Experimental and theoretical investigation of the mass transfer controlled regime in catalytic monoliths. *Catalysis Today*, Volume 88, Issues 1-2, 2003, Pages 3-16.

[21] J. Davies, D. Maynes, B.W. Webb, and B. Woolford. Laminar flow in a microchannel with superhydrophobic walls exhibiting transverse ribs. *Physics of Fluids*, Volume 18, Issue 8, 2006, Article Number: 087110.

[22] D. Maynes, K. Jeffs, B. Woolford, and B.W. Webb. Laminar flow in a microchannel with hydrophobic surface patterned microribs oriented parallel to the flow direction. *Physics of Fluids*, Volume 19, Issue 9, 2007, Article Number: 093603.

[23] S. Ogo and Y. Sekine. Recent progress in ethanol steam reforming using non-noble transition metal catalysts: A review. *Fuel Processing Technology*, Volume 199, 2020, Article Number: 106238.

[24] T.L. LeValley, A.R. Richard, and M. Fan. The progress in water gas shift and steam reforming hydrogen production technologies - A review. *International Journal of Hydrogen Energy*, Volume 39, Issue 30, 2014, Pages 16983-17000.

[25] C.J. Jiang, D.L. Trimm, M.S. Wainwright, and N.W. Cant. Kinetic study of steam reforming of methanol over copper-based catalysts. *Applied Catalysis A: General*, Volume 93, Issue 2, 1993, Pages 245-255.

[26] K. Takahashi, N. Takezawa, and H. Kobayashi. The mechanism of steam reforming of methanol over a copper-silica catalyst. *Applied Catalysis*, Volume 2, Issue 6, 1982, Pages 363-366.

[27] G.A. Olah. Beyond oil and gas: The methanol economy. *Angewandte Chemie International Edition*, Volume 44, Issue 18, 2005, Pages 2636-2639.

[28] F.J. Keil. Methanol-to-hydrocarbons: Process technology. *Microporous and Mesoporous Materials*, Volume 29, Issues 1-2, 1999, Pages 49-66.

[29] N. Edwards, S.R. Ellis, J.C. Frost, S.E. Golunski, A.N.J. van Keulen, N.G. Lindewald, and J.G. Reinkingh. On-board hydrogen generation for transport applications: The HotSpot™ methanol processor. *Journal of Power Sources*, Volume 71, Issues 1-2, 1998, Pages 123-128.

[30] C. Rameshan, W. Stadlmayr, S. Penner, H. Lorenz, N. Memmel, M. Hävecker, R. Blume, D. Teschner, T. Rocha, D. Zemlyanov, A. Knop-Gericke, R. Schlögl, and B. Klötzer. Hydrogen production by methanol steam reforming on copper boosted by zinc-assisted water activation. *Angewandte Chemie International Edition*, Volume 51, Issue 12, 2012, Pages 3002-3006.

[31] M.F.N. D'Angelo, V. Ordomsky, J. van der Schaaf, J.C. Schoutena, and T.A. Nijhuis. Aqueous phase reforming in a microchannel reactor: the effect of mass transfer on hydrogen selectivity. *Catalysis Science & Technology*, Volume 3, Issue 10, 2013, Pages 2834-2842.

[32] Y. Chen, F. Yao, and X. Huang. Mass transfer and reaction in methanol steam reforming reactor with fractal tree-like microchannel network. *International Journal of Heat and Mass Transfer*, Volume 87, 2015, Pages 279-283.

[33] C.-Y. Hsueh, H.-S. Chu, W.-M. Yan, C.-H. Chen, and M.-H. Chang. Numerical study of heat and mass transfer in the plate methanol steam micro-reformer channels. *Applied Thermal Engineering*, Volume 30, Issues 11-12, 2010, Pages 1426-1437.

[34] F. Yao, Y. Chen, and G.P. Peterson. Hydrogen production by methanol steam reforming in a disc microreactor with tree-shaped flow architectures. *International Journal of Heat and Mass Transfer*, Volume 64, 2013, Pages 418-425.

[35] J. Bode. Computational fluid dynamics applications in the chemical industry. *Computers & Chemical Engineering*, Volume 18, Supplement 1, 1994, Pages S247-S251.

[36] J.A.M. Kuipers and W.P.M. van Swaaij. Computational fluid dynamics applied to chemical reaction engineering. *Advances in Chemical Engineering*, Volume 24, 1998, Pages 227-328.

[37] J.D. Wilde and G.F. Froment. Computational fluid dynamics in chemical reactor analysis and design: Application to the ZoneFlow™ reactor for methane steam reforming. *Fuel*, Volume 100, 2012, Pages 48-56.

[38] A.G. Dixon, M. Nijemeisland, and E.H. Stitt. Packed tubular reactor modeling and catalyst design using computational fluid dynamics. *Advances in Chemical Engineering*, Volume 31, 2006, Pages 307-389.

[39] M.A. Ashraf, O. Sanz, M. Montes, and S. Specchia. Insights into the effect of catalyst loading on methane steam reforming and controlling regime for metallic catalytic monoliths. *International Journal of Hydrogen Energy*, Volume 43, Issue 26, 2018, Pages 11778-11792.

[40] A. Jeong, D. Shin, S.M. Baek, and J.H. Nam. Effectiveness factor correlations from simulations of washcoat nickel catalyst layers for small-scale steam methane reforming applications. *International Journal of Hydrogen Energy*, Volume 43, Issue 32, 2018, Pages 15398-15411.

[41] H. Nourbakhsh, J.R. Shahrouzi, H. Ebrahimi, A. Zamaniyan, and M.R.J. Nasr. Experimental and numerical study of syngas production during premixed and ultra-rich partial oxidation of methane in a porous reactor. *International Journal of Hydrogen Energy*, Volume 44, Issue 60, 2019, Pages 31757-31771.

[42] H.E. Figen and S.Z. Baykara. Effect of ruthenium addition on molybdenum catalysts for syngas production via catalytic partial oxidation of methane in a monolithic reactor. *International Journal of Hydrogen Energy*, Volume 43, Issue 2, 2018, Pages 1129-1138.

[43] B.A. Peppley, J.C. Amphlett, L.M. Kearns, and R.F. Mann. Methanol-steam reforming on Cu/ZnO/Al_2O_3. Part 1: the reaction network. *Applied Catalysis A: General*, Volume 179, Issues 1-2, 1999, Pages 21-29.

[44] T.L. Reitz, S. Ahmed, M. Krumpelt, R. Kumar, and H.H. Kung. Characterization of CuO/ZnO under oxidizing conditions for the oxidative methanol reforming reaction. *Journal of Molecular Catalysis A: Chemical*, Volume 162, Issues 1-2, 2000, Pages 275-285.

[45] S. Sá, H. Silva, L. Brandão, J.M. Sousa, and A. Mendes. Catalysts for methanol steam reforming-A review. *Applied Catalysis B: Environmental*, Volume 99, Issues 1-2, 2010, Pages 43-57.

[46] *ANSYS FLUENT user's guide*, Release 18.1, ANSYS Inc., Canonsburg, Pennsylvania, United States, 2017.

[47] J.H. Nam. Effectiveness factor correlations for spherical nickel catalyst pellets used in small-scale steam methane reformers. *International Journal of Hydrogen Energy*, Volume 40, Issue 16, 2015, Pages 5644-5652.

[48] T.P.K. Sidhu and S. Roy. Optimal design of washcoated monolith catalyst for compact, heat-integrated ethanol reformers. *International Journal of Hydrogen Energy*, Volume 44, Issue 23, 2019, Pages 11472-11487.

[49] A. Jeong, D. Shin, S.M. Baek, and J.H. Nam. Effectiveness factor correlations from simulations of washcoat nickel catalyst layers for small-scale steam methane reforming applications. *International Journal of Hydrogen Energy*, Volume 43, Issue 32, 2018, Pages 15398-15411.

[50] C. Cao, N. Zhang, D. Dang, and Y. Cheng. Hybrid modeling of integrated microchannel methane reformer for miniaturized GTL application using an effectiveness factor submodel based on complex surface chemistry. *Chemical Engineering Journal*, Volume 316, 2017, Pages 715-726.

[51] D.B. Ingham and I. Pop. *Transport Phenomena in Porous Media*, Elsevier Science Ltd., Oxford, the United Kingdom, 1998, ISBN: 978-0-08-042843-7.

[52] B.D. Eldridge and L.F. Brown. The effect of cross sectional pore shape on Knudsen diffusion in porous materials. *AIChE Journal*, Volume 22, Issue 5, 1976, Pages 942-944.

[53] A.F. Wagner. The challenges of combustion for chemical theory. *Proceedings of the Combustion Institute*, Volume 29, Issue 1, 2002, Pages 1173-1200.

[54] E. Shustorovich and H. Sellers. The UBI-QEP method: A practical theoretical approach to understanding chemistry on transition metal surfaces. *Surface Science Reports*, Volume 31, Issues 1-3, 1998, Pages 1-119.

[55] E.R. Ritter and J.W. Bozzelli. THERM: Thermodynamic property estimation for gas phase radicals and molecules. *International Journal of Chemical Kinetics*, Volume 23, Issue 9, 1991, Pages 767-778.

[56] E.S. Blurock, V. Warth, X. Grandmougin, R. Bounaceur, P.-A. Glaude, and F. Battin-Leclerc. JTHERGAS: Thermodynamic estimation from 2D graphical representations of molecules. *Energy*, Volume 43, Issue 1, 2012, Pages 161-171.

[57] D.R. Palo, R.A. Dagle, and J.D. Holladay. Methanol steam reforming for hydrogen production. *Chemical Reviews*, Volume 107, Issue 10, 2007, Pages 3992-4021.

[58] S.T. Yong, C.W. Ooi, S.P. Chai, and X.S. Wu. Review of methanol reforming-Cu-based catalysts, surface reaction mechanisms, and reaction schemes. *International Journal of Hydrogen Energy*, Volume 38, Issue 22, 2013, Pages 9541-9552.

[59] B.A. Peppley, J.C. Amphlett, L.M. Kearns, and R.F. Mann. Methanol-steam reforming on Cu/ZnO/Al_2O_3 catalysts. Part 2. A comprehensive kinetic model. *Applied Catalysis A: General*, Volume 179, Issues 1-2, 1999, Pages 31-49.

[60] S.P. Asprey, B.W. Wojciechowski, and B.A. Peppley. Kinetic studies using temperature-scanning: the steam-reforming of methanol. *Applied Catalysis A: General*, Volume 179, Issues 1-2, 1999, Pages 51-70.

[61] F.L. Dryer, F.M. Haas, J. Santner, T.I. Farouk, and M. Chaos. Interpreting chemical kinetics from complex reaction-advection-diffusion systems: Modeling of flow reactors and related experiments. *Progress in Energy and Combustion Science*, Volume 44, 2014, Pages 19-39.

[62] G.-G. Park, D.J. Seo, S.-H. Park, Y.-G. Yoon, C.-S. Kim, and W.-L. Yoon. Development of microchannel methanol steam reformer. *Chemical Engineering Journal*, Volume 101, Issues 1-3, 2004, Pages 87-92.

[63] J.P. Lopes, M.A. Alves, M.S.N. Oliveira, S.S.S. Cardoso, and A.E. Rodrigues. Regime mapping and the role of the intermediate region in wall-coated microreactors. *Chemical Engineering Science*, Volume 94, 2013, Pages 166-184.

[64] J.M. Blasi, P.J. Weddle, C. Karakaya, D.R. Diercks, and R.J. Kee. Modeling reaction-diffusion processes within catalyst washcoats: II. Macroscale processes informed by microscale simulations. *Chemical Engineering Science*, Volume 145, 2016, Pages 308-316.

[65] J.P. Lopes, S.S.S. Cardoso, and A.E. Rodrigues. Criteria for kinetic and mass transfer control in a microchannel reactor with an isothermal first-order wall reaction. *Chemical Engineering Journal*, Volumes 176-177, 2011, Pages 3-13.

[66] J.P. Lopes, S.S.S. Cardoso, and A.E. Rodrigues. Interplay between channel and catalyst operating regimes in wall-coated microreactors. *Chemical Engineering Journal*, Volume 227, 2013, Pages 42-55.

[67] R.E. Hayes and S.T. Kolaczkowski. Mass and heat transfer effects in catalytic monolith reactors. *Chemical Engineering Science*, Volume 49, Issue 21, 1994, Pages 3587-3599.

[68] S.T. Kolaczkowski. Modelling catalytic combustion in monolith reactors - challenges faced. *Catalysis Today*, Volume 47, Issues 1-4, 1999, Pages 209-218.

[69] S. Han and R.J. Goldstein. The heat/mass transfer analogy for a simulated turbine endwall.

International Journal of Heat and Mass Transfer, Volume 51, Issues 11-12, 2008, Pages 3227-3244.

[70] S. Han and R.J. Goldstein. The heat/mass transfer analogy for a simulated turbine blade. *International Journal of Heat and Mass Transfer*, Volume 51, Issues 21-22, 2008, Pages 5209-5225.

[71] W.M. Kays and M.E. Crawford. *Convective Heat and Mass Transfer*, third Edition, McGraw-Hill Publishing Company, Inc., New York City, the United States, 1993, ISBN: 978-0-07-033721-3.

[72] E.R.G. Eckert and R.M. Drake. *Analysis of Heat and Mass Transfer*, McGraw-Hill Publishing Company, Inc., New York City, the United States, 1972, ISBN: 978-0-07-018925-6.

[73] T.L. Bergman, A.S. Lavine, F.P. Incropera, and D.P. DeWitt. *Fundamentals of Heat and Mass Transfer*, 8th Edition, John Wiley & Sons, Inc., Hoboken, New Jersey, the United States, 2018, ISBN: 978-1-119-35388-1.

[74] J. Welty, G.L. Rorrer, and D.G. Foster. *Fundamentals of Momentum, Heat, and Mass Transfer*, 7th Edition, John Wiley & Sons, Inc., Hoboken, New Jersey, the United States, 2019, ISBN: 978-1-119-49541-3.

[75] R.-Y. Chein, L.-C. Chen, Y.-C. Chen, and J.N. Chung. Heat transfer effects on the methanol-steam reforming with partially filled catalyst layers. *International Journal of Hydrogen Energy*, Volume 34, Issue 13, 2009, Pages 5398-5408.

[76] D. Merino, O. Sanz, and M. Montes. Effect of the thermal conductivity and catalyst layer thickness on the Fischer-Tropsch synthesis selectivity using structured catalysts. *Chemical Engineering Journal*, Volume 327, 2017, Pages 1033-1042.

[77] R.H. Venderbosch, W. Prins, and W.P.M. van Swaaij. Platinum catalyzed oxidation of carbon monoxide as a model reaction in mass transfer measurements. *Chemical Engineering Science*, Volume 53, Issue 19, 1998, Pages 3355-3366.

[78] R. Aris. Mass transfer from small ascending bubbles. *Chemical Engineering Science*, Volume 52, Issue 24, 1997, Pages 4439-4446.